

Coherently controlled ionization of gases by three-color femtosecond laser pulsesShixiang Wang^{1,*}, Chenhui Lu^{2,*}, Zhengquan Fan,¹ Aurélien Houard,³ Vladimir Tikhonchuk^{4,5}, André Mysyrowicz,³ Songlin Zhuang,¹ Vasily A. Kostin,^{6,7,†} and Yi Liu^{1,8,‡}¹*Shanghai Key Lab of Modern Optical System, University of Shanghai for Science and Technology, Engineering Research Center of Optical Instrument and System, The Ministry of Education, 516, Jungong Road, 200093 Shanghai, China*²*School of Mechanical and Automotive Engineering, Shanghai University of Engineering Science, Shanghai 201620, China*³*Laboratoire d'Optique Appliquée, ENSTA Paris, CNRS, Ecole Polytechnique, Institut Polytechnique de Paris, 828 Boulevard des Maréchaux, 91762 Palaiseau cedex, France*⁴*Centre Lasers Intenses et Applications, Université de Bordeaux–CNRS–CEA, 351 Cours de la Libération, 33405 Talence cedex, France*⁵*ELI-Beamlines Center, Institute of Physics, Czech Academy of Sciences, 25241 Dolní Břežany, Czech Republic*⁶*Institute of Applied Physics, Russian Academy of Sciences, Nizhny Novgorod 603950, Russia*⁷*University of Nizhny Novgorod, Nizhny Novgorod 603950, Russia*⁸*CAS Center for Excellence in Ultra-Intense Laser Science, Shanghai 201800, China*

(Received 26 September 2021; revised 28 January 2022; accepted 7 February 2022; published 28 February 2022)

Photoionization of atoms and molecules by intense femtosecond laser pulses is a fundamental process of strong-field physics. Using a three-color femtosecond laser scheme with attosecond phase control precision, we demonstrate coherently controlled ionization of nitrogen molecules with a modulation level up to 45% by varying the phase shifts between the fundamental laser frequency at 800 nm and its second and third harmonics. Furthermore, the phase dependence of the ionization degree qualitatively changes with the laser intensity ratios between the three colors. The observations are interpreted as a manifestation of the competition between different parametric channels contributing to the ionization process. Such coherent control of ionization opens different ways to finely tune and optimize various phenomena accompanying laser-material interactions: high-order harmonic and attosecond generation, nanofabrication, remote ablation of samples, and even guidance of discharge and control of lightning by lasers.

DOI: [10.1103/PhysRevA.105.023529](https://doi.org/10.1103/PhysRevA.105.023529)

Photoionization of atoms and molecules lays the foundation for strong-field physics effects including the generation of high-order harmonics (HHG) and attosecond pulses [1], long-distance filamentary propagation of intense ultrashort pulses [2,3], emission of microwave to terahertz (THz) electromagnetic waves [4,5], micro- and nanomachining of dielectrics [6], remote ablation of samples [7], etc. For all these effects, the ionization rate and the corresponding final electron density are key parameters, and therefore, their proper control is highly desirable. With a single-color pulse, adaptive temporal pulse shape control has the capacity to enhance or suppress ionization of certain atoms or molecules, a process that is usually based on energy level resonance [8–12]. Moreover, it has been demonstrated that ionization of molecules can be enhanced and coherently controlled with two-color laser pulses composed of a fundamental frequency with either its second or third harmonics [13–15]. Recently, it has been reported that a laser field composed of three or more colors can be even more beneficial [16–19]. Compared to two-color laser field excitation, the three-color scheme provides extra control parameters and has proven its versatility in the selection of

single harmonic radiation from the comb of high-order harmonics [20], in the coherent control of the polarization and chirality of THz pulses produced from air plasma [19], and in the generation of supercontinuum ranging from midinfrared to ultraviolet [18,21]. However, the fundamental process of molecule ionization by a phase-controlled three-color laser field has remained largely unexplored.

In the present study, we demonstrate both experimentally and theoretically, using ambient air as an example, that the tunnel ionization of molecular gases can be coherently controlled by laser pulses composed of the fundamental frequency and its second and third harmonics. We find that the ionization degree of the formed plasma, monitored by its fluorescence, changes periodically when the phase shifts between the three harmonics are varied. Interestingly, it is also found that the ionization rate presents different dependencies on the phases for different intensity ratios between the three colors of the laser field. The interpretation of the experimental results is based on the concept that different ionization channels contribute to electron tunneling in strong multicolor fields. The competition between the three different parametric channels is manifested through the complex phase dependencies of the ionization rate. For different intensity ratios between the three colors, the dominating parametric channels of ionization changes, in agreement with the experimentally observed intensity-dependent phase graphs. These findings provide a

*These authors contributed equally to this work.

†vk1@ipfran.ru

‡yi.liu@usst.edu.cn

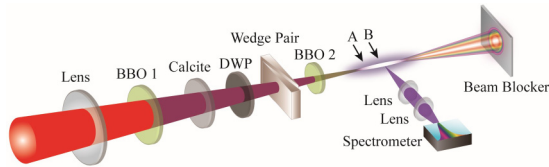


FIG. 1. Schematic experimental setup is presented. The fluorescence of the air plasma was collected by two lenses of $f = 20$ mm and 35 mm into the fiber tip and analyzed by a spectrometer. The two arrows indicate locations A and B, from where the fluorescence was collected and analyzed.

robust and simple method for enhancing and controlling the ionization of atoms and molecules, which is of great significance for strong-field physics as well as nonlinear optics.

We used an in-line three-color femtosecond laser pulse to create a plasma filament in ambient air. The three-color pulse is composed of a fundamental field at 800 nm and its second and third harmonics. The experimental setup is schematically shown in Fig. 1. Femtosecond laser pulses of $\tau_p = 35$ fs duration with a central wavelength $\lambda = 800$ nm are focused in ambient air by a lens with focal length $f = 500$ mm. A $200\text{-}\mu\text{m}$ -thick type I beta barium borate (β -BBO) crystal cut at 29.2° is used for second harmonic generation with a wavelength $\lambda_{400} = 400$ nm, followed by a calcite to compensate for the time delay between the 800 - and 400 -nm pulses. A dual-wavelength waveplate, which rotates the polarization of the 800 -nm pulse from the vertical to horizontal direction while leaving the polarization of 400 nm unchanged, is used to adjust the polarization status of the pulses. A pair of fused silica wedges is used to finely tune the temporal delay $\Delta\tau$ and phases $\Delta\phi$ between the 400 - and 800 -nm pulses. The phase variation between the 800 - and 400 -nm pulses introduced by insertion of the wedge reads as $\Delta\phi = 2\pi(n_{800}^{\text{FS}} - n_{400}^{\text{FS}}) \frac{\Delta d}{\lambda_{400}} \tan \theta$, where n_{800}^{FS} and n_{400}^{FS} are the refractive indices of fused silica for 800 and 400 nm, respectively, and Δd and θ are the change in transverse insertion and angle of the fused silica wedge. Considering that $\theta = 3^\circ$ in our experiment, the phase $\Delta\phi$ between 800 and 400 nm can be precisely changed by 0.044π for an increment of Δd by

$10 \mu\text{m}$. The third harmonic at the wavelength $\lambda_{266} = 266$ nm is generated by using another $50\text{-}\mu\text{m}$ -thick type I beta barium borate (β -BBO) crystal cut at 44.3° . It was experimentally found that after this BBO crystal, the 800 -, 400 -, and 266 -nm beam become elliptically polarized with their major components in the vertical direction, as presented in Fig. 2. By displacing BBO 2 with respect to the laser focus, the relative phase $\Delta\gamma$ between 266 and 400 nm can be changed according to $\Delta\gamma = 2\pi(n_{400}^{\text{air}} - n_{266}^{\text{air}})\Delta l/\lambda_{266}$, where n_{400}^{air} and n_{266}^{air} are the refractive indices of air for 400 and 266 nm, respectively, and Δl is the distance between BBO 2 and the laser geometrical focus. Therefore, $\Delta\gamma$ can be finely tuned by 0.0011π as Δl changes by $10 \mu\text{m}$. With this in-line setup for three-color laser field synthesis, one can readily control the phases between the different optical frequencies with attosecond precision [19]. For an incident 800 -nm pulse energy of $\sim 1\text{--}2$ mJ, a bright plasma filament with a length of $30\text{--}50$ mm is formed in ambient air. Two fused silica lenses with focal lengths of 20 and 35 mm were used to collect the fluorescence signal into an optical fiber connected to a spectrometer (ARC-SP-2758, PI). We collected the fluorescence signal from a filament segment length of 1 mm, which was realized by a slit installed between the filament and the collimation lens.

A typical emission spectrum of the air plasma filament is shown in Fig. 3(a). The observed lines correspond to transitions between excited triplet states $C^3\Pi_u^+$ and $B^3\Pi_g^+$ of neutral nitrogen molecules (the second positive system of N_2) and between the second excited state $B^2\Sigma_u^+$ and ground state $X^2\Sigma_g^+$ of nitrogen molecular ions (the first negative system of N_2^+) [22]. In Fig. 3(a), the corresponding transitions are indicated. The emission of nitrogen ions at 391.4 nm corresponds to the electronic transition from the HOMO-2 orbital to the highest occupied molecular orbital (HOMO). Therefore, its spectral intensity reflects the population density of nitrogen ions in the $B^2\Sigma_u^+$ state. Regarding the emission from neutral nitrogen molecules, it is known that the upper molecular state $C^3\Pi_u^+$ becomes occupied through collisional excitation of nitrogen molecules in the ground state $X^1\Sigma_g^+$ with energetic electrons [22,23]. Therefore, the corresponding line intensities are linearly proportional to the electron concentration inside the plasma, which under our experimental conditions is expected

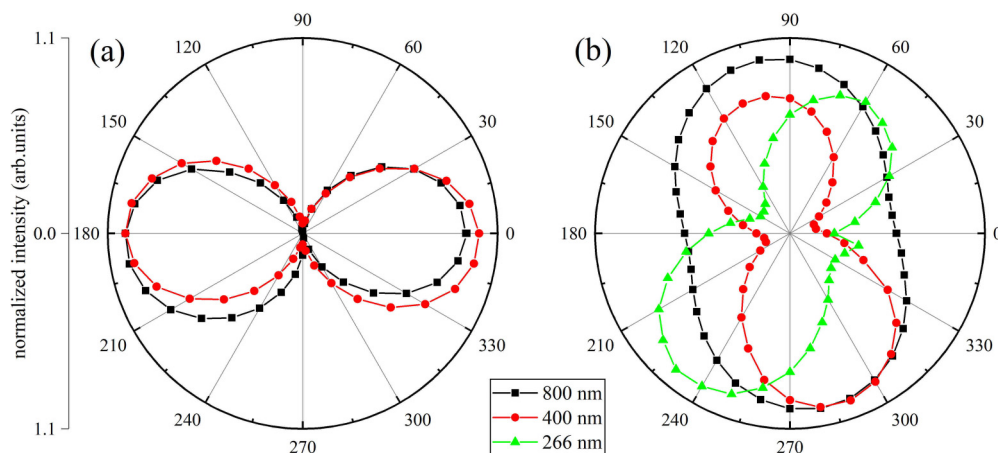


FIG. 2. Measured polarization of the optical fields before (a) and after (b) the sum frequency generation BBO crystal.

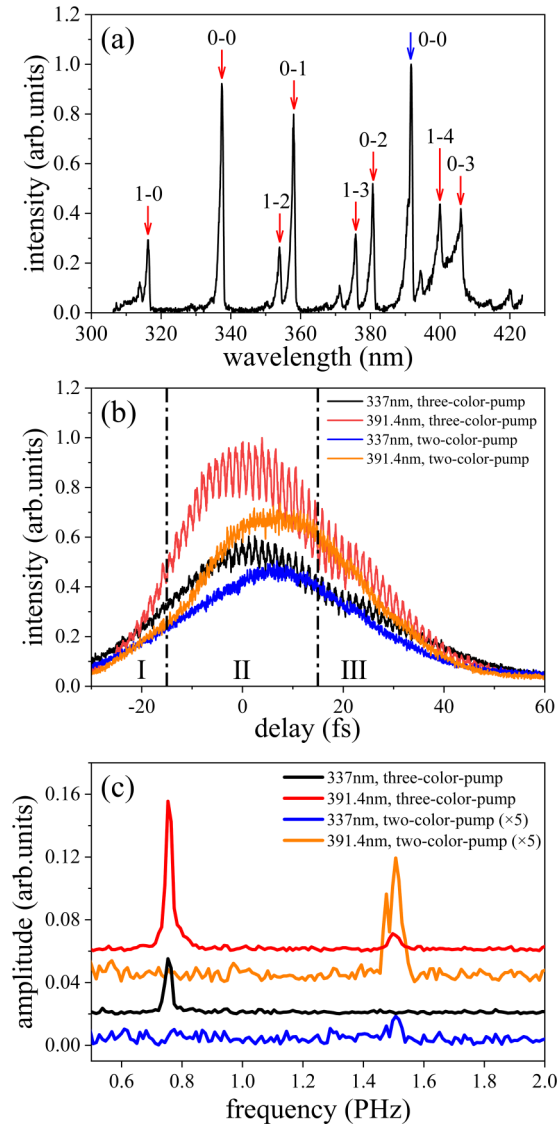


FIG. 3. (a) Emission spectrum of the air plasma. The spectral peaks stem from transitions between different energy levels of N_2 and N_2^+ . The related vibrational quantum numbers of the upper and lower levels of the second positive band of N_2 (red arrow) and first negative band of N_2^+ (blue arrow) are indicated. (b) The 337- and 391.4 nm fluorescence as a function of the phase shift $\Delta\varphi$ between the second harmonic and fundamental field (proportional to the temporal delay $\Delta\tau$ introduced by the wedge pair), in case of two-color and three-color pumping. The pulse energy of the 800-nm pump laser is 1.8 mJ. (c) The Fourier transform of the signals in (b).

to be mostly determined by the concentration of oxygen ions due to lower ionization potential of oxygen molecule as compared to nitrogen. Here, we select the 337- and 391.4-nm lines for monitoring, which represent the production of free electrons and nitrogen ions, respectively.

In Fig. 3(b), we present the dependence of the 391.4- and 337-nm signals when the optical wedge thickness is continuously increased in the optical beam path. A positive delay corresponds to a 400-nm pulse arriving after the 800-nm pulse. The signals increase and decrease upon scanning of the optical wedge, reflecting the transitory temporal overlap of

the 800- and 400-nm pulses, which results in third harmonic generation at 266 nm. More importantly, a modulation with a period of ~ 1.3 fs is noticeable, which indicates coherent ionization control determined by the phase $\Delta\varphi$ between 800 and 400 nm. A maximum modulation depth of $\sim 20\%$ is routinely observed in the experiments. For comparison, we also present the results obtained with 800- and 400-nm laser fields, where the modulation is barely observable. This illustrates the advantage of the three-color fields over the two-color case. The Fourier transformation of the signals in Fig. 3(b) is presented in Fig. 3(c). In case of three-color pumping, this transformation yields a main peak at 0.75 PHz (corresponding to the temporal period of 1.3 fs or the period 2π in phase $\Delta\varphi$) and a secondary peak at 1.49 PHz (corresponding to the temporal period 0.67 fs or the phase period of π). For two-color case, only one peak at 1.49 PHz is observed. Their origin and difference will be discussed later.

We then investigated the influence of both $\Delta\varphi$ and $\Delta\gamma$ on the ionization rate. In the experiments, different laser intensity ratios of the three optical frequencies were examined. To study the effect of relative intensity changes between the three optical fields at 800, 400, and 266 nm, we performed measurements of the plasma fluorescence (a) at different locations along the long filament (point A or B in Fig. 1), (b) by changing the partial or total temporal overlap between the three colors [Fig. 3(b)], or (c) by changing the incident 800-nm pulse energy. The fluence and corresponding averaged laser intensity of the three optical fields inside the filaments were calculated using the method involving an *in situ* filament-drilled pinhole, which provides a measurement of the average laser fluence within a diameter of ~ 90 μm in the current experiments [24,25]. The measured diameter of the filament-drilled pinhole and the laser fluence of the three wavelengths are summarized in Table I.

In the first experiment, we measured the fluorescence at the front of the plasma (location A in Fig. 1) with a partial overlap of the 400-nm pulses with the main 800-nm pulses [stage I in Fig. 3(b)]. The ratio of intensities $I^{(400)}/I^{(800)}$ was then estimated to be 0.049. The measured dependence of the 337 nm signal on both $\Delta\varphi$ and $\Delta\gamma$ is shown in Fig. 4(a) in the form of a two-dimensional (2D) phase diagram. The corresponding result for the 391.4-nm fluorescence is presented in Fig. 5(a). Here, the maximum ionization signal remains approximately constant, and the peaks in the 2D phase diagram shift continuously upon an increase in both $\Delta\varphi$ and $\Delta\gamma$. In other words, a constant $\Delta\varphi + \Delta\gamma$ gives rise to a rather constant ionization rate. We next moved to the middle of the filament (location B in Fig. 1) and performed the measurement around a good temporal overlap between the 400- and 800-nm pulses [stage II in Fig. 3(b)]. In this case, the incident 800-nm pulse energy was 0.65 mJ. The intensity ratio $I^{(400)}/I^{(800)}$ was estimated to be 0.163. The corresponding results for 337- and 391.4-nm fluorescence are presented in Figs. 4(b) and 5(b). Here, the maximum ionization is achieved at some isolated regions in the 2D phase diagram; i.e., a “chessboard” pattern is observed. In the third case, the intensity ratio $I^{(400)}/I^{(800)}$ was further increased to 0.397 by increasing the incident 800-nm pulse energy to 1.88 mJ. The corresponding results are shown in Figs. 4(c) and 5(c). Now, the maximum ionization remains rather constant again, while the peaks shift gradually

TABLE I. The measured laser fluence inside the filament for three cases in the experiments.

	Wavelength (nm)	Pinhole diameter (μm)	Laser energy through the pinhole (μJ)	Calculated averaged fluence (J/cm^2)	Calculated maximal intensity (W/cm^2)	Intensity ratio
Case I	800	103.594	482.600	1.431	7.687E+13	1
	400	104.048	237.723	0.070	3.760E+12	0.049
	266	102.323	3.959	0.012	6.446E+11	0.008
Case II	800	92.901	303.800	1.120	6.016E+13	1
	400	92.504	48.948	0.182	9.776E+12	0.163
	266	93.871	1.486	0.005	2.686E+11	0.005
Case III	800	100.230	438.800	1.390	7.466E+13	1
	400	102.075	180.828	0.552	2.965E+13	0.397
	266	102.776	7.769	0.023	1.235E+12	0.017

for a constant $\Delta\varphi - \Delta\gamma$. One can notice that the modulation depth of ionization becomes 40% in Fig. 4(c) and 45% in Fig. 5(c). To obtain further insight into the 2D phase dependence of Figs. 4(a)–4(c) and 5(a)–5(c), we performed 2D Fourier transformation. The corresponding results are shown in Figs. 4(d)–4(f) and 5(d)–5(f). A series of peaks are observed in the frequency map, with different peaks dominating the three regions of the intensity ratio $I^{(400)}/I^{(800)}$. As will be discussed, these peaks correspond to the different parametric channels involved for tunneling ionization.

Control of photoionization can enable broad applications in the domain of laser-material interactions. As an example, here we present how the starting position and the fluorescence intensity of the femtosecond laser filaments can be manipulated, as shown in Fig. 6. In Fig. 6(a), we show an image of the plasma filament created by the three-color laser fields.

By varying the phase $\Delta\varphi$ the starting point of the filament (SPOF) is observed to change periodically, as presented in Fig. 6(b). Moreover, the fluorescence signal integrated in the whole visible light range at two fixed positions in the leading and middle sections of the filament [indicated by the arrows in Fig. 6(a)] is found to present oscillatory behavior, resulting from the modulation of the ionization degree of air molecules. In addition to the starting point and the electron density of the filament, it is natural to expect that other parameters of the filaments, such as the clamping laser intensity, white light generation, and secondary radiation (terahertz and microwave radiation), can be controlled. Considering that this method of coherently controlling ionization is general and does not rely on the internal structure (such as the energy level) of the gas particles, we believe that it can find wide applications in many contemporary frontiers of strong-field physics

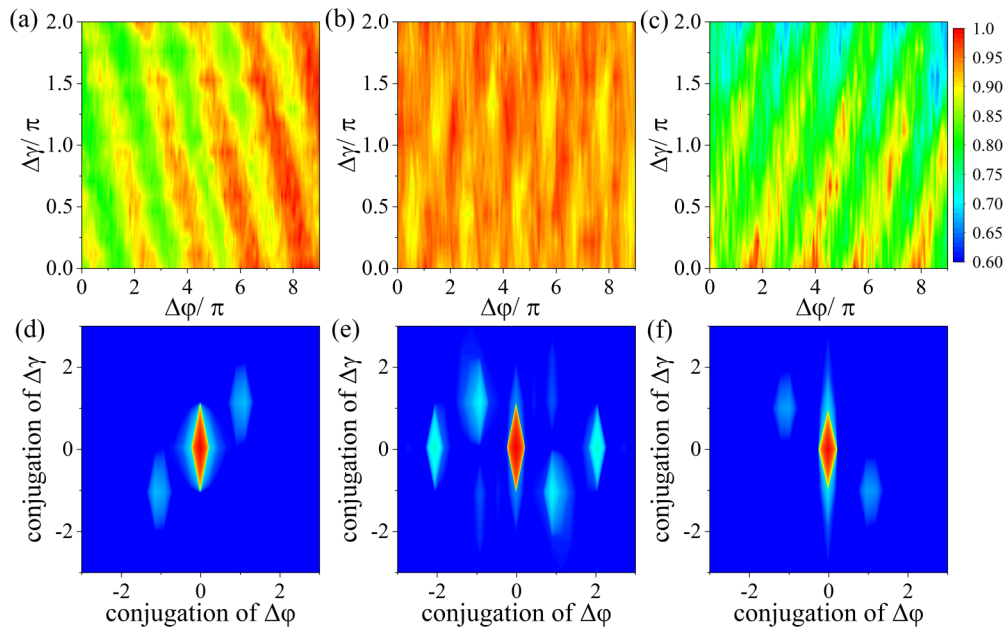


FIG. 4. Dependence of the 337-nm fluorescence signal on the relative phases $\Delta\varphi$ and $\Delta\gamma$ and its Fourier transformation. (a) The signals are collected at the front side of the plasma (location A in Fig. 1) and at the rising edge in Fig. 3(b). The pump pulse energy is 1.88 mJ. (b) The signals are collected in the middle of the plasma (location B) and at the summit of Fig. 3(b). The pump energy is 0.65 mJ. (c) The signals are collected at the front edge of the plasma (location A in Fig. 1) and at the summit of Fig. 3(b). The pump pulse energy is 1.88 mJ. (d)–(f), The normalized 2D Fourier transform (logarithmic scale) of the experimental signals on the top.

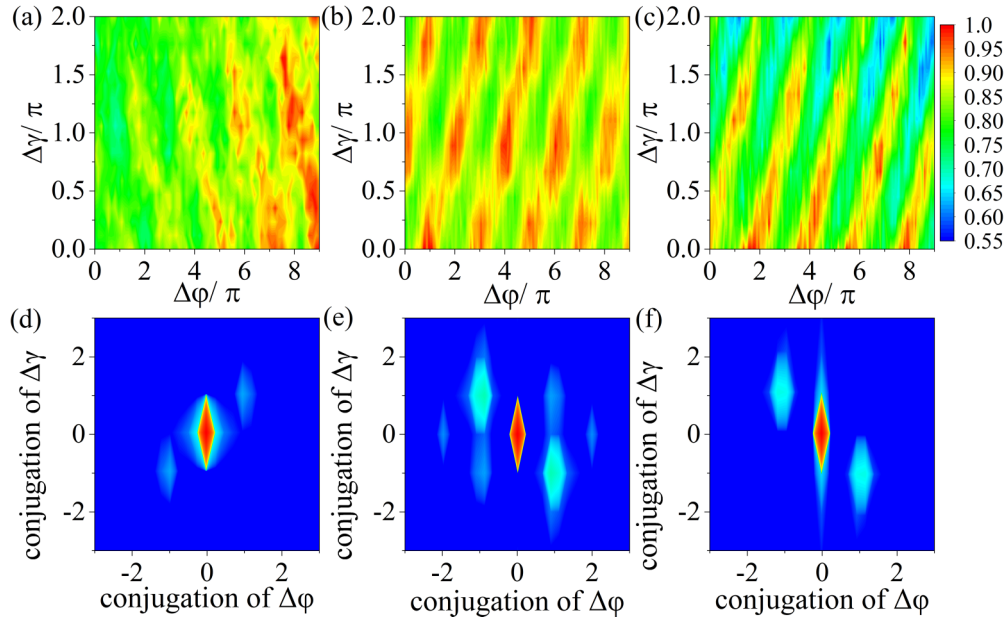


FIG. 5. The 391.4-nm fluorescence signal as a function of the phases $\Delta\phi$ and $\Delta\gamma$. (a) The signals were collected at the front side of the plasma and at the rising edge in Fig. 3(b). The pump pulse energy is 0.65 mJ. (b) The signals were obtained at the middle of plasma and at the summit of Fig. 3(b). The pump energy is 0.65 mJ. (c) The signals were collected at the front edge of the plasma and at the summit of Fig. 3(b). The pump pulse energy is 1.88 mJ. (d)–(f), The normalized 2D Fourier transform (logarithmic scale) of the signals on the top.

where photoionization is crucial, such as high-order harmonic generation and attosecond science [1], nanofabrication with

femtosecond pulses [6], remote ablation of samples by intense laser pulses [7], and even guiding of discharge and control of lightning by lasers [3].

To explain the results of the experiment, we calculated the plasma density produced in the tunnel ionization of gas molecules by the three-color linearly polarized electric field $\mathbf{E}(t) = E(t)\hat{\mathbf{x}}$,

$$E(t) = F(t)[\mathcal{E}_{800} \cos(\omega_{800}t) + \mathcal{E}_{400} \cos(2\omega_{800}t + \varphi) + \mathcal{E}_{266} \cos(3\omega_{800}t + \varphi + \gamma)]. \quad (1)$$

Here, $F(t) = e^{-2\ln^2(t/\tau_p)}$ is the pulse envelope, τ_p is the intensity full width at half maximum, $\mathcal{E}_{800, 400, 266} = \sqrt{2I^{(800, 400, 266)}/c\epsilon_0}$ are the peak amplitudes of the fundamental, second, and third harmonics, $I^{(800, 400, 266)}$ are their peak intensities, c is the speed of light, ϵ_0 is the vacuum permittivity, $\omega_{800} = 2\pi c/\lambda_{800}$ is the fundamental frequency, φ is the phase shift between the second and fundamental harmonics, and γ is the phase shift between the third and second harmonics. The time-varying plasma density $N(t)$ satisfies the ionization equation $\partial N/\partial t = (N_g - N)w(|E|)$ with zero initial condition at time $t \rightarrow -\infty$, where N_g is the initial concentration of neutral particles, and $w(|E|)$ is the tunnel ionization probability per unit time in the static electric field.

To obtain an analytical expression for the period-averaged ionization probability in the three-color field (1), we employ the multiwave mixing approach similar to that proposed in [26]. Since the field (1) is 2π periodic with respect to phases $\psi_{800} = \omega_{800}t$, $\psi_{400} = 2\omega_{800}t + \varphi$, and $\psi_{266} = 3\omega_{800}t + \varphi + \gamma$, the instantaneous ionization probability $w(|E|)$ is also periodic and can be decomposed in the triple Fourier

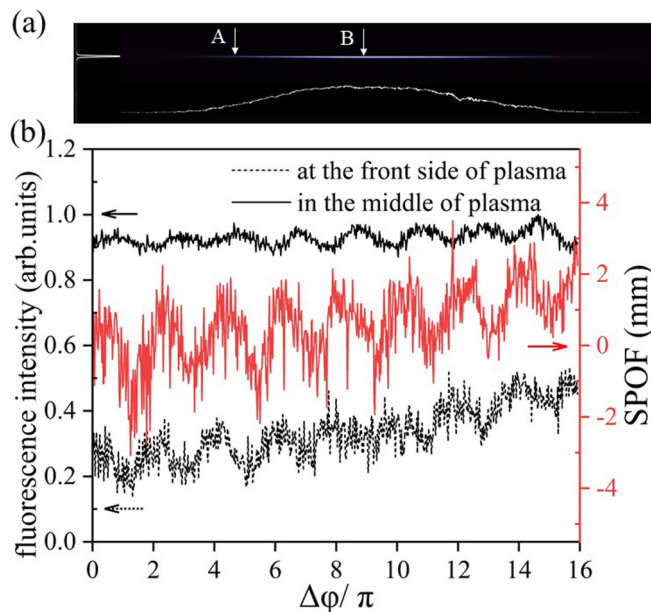


FIG. 6. Coherent control of the starting position and fluorescence of the femtosecond filament in air. (a) Image of the plasma filament in air. The three-color pump pulses propagate from left to right. The curves on the left and bottom sides correspond to the distribution of the fluorescence intensity in the longitudinal and transverse directions. (b) Fluorescence intensities at two positions [indicated by the arrows in (a)] and the starting position of the filament (SPOF) as a function of the phase $\Delta\phi$.

series

$$w(|E|) = \sum_{p=-\infty}^{\infty} \sum_{q=-\infty}^{\infty} \sum_{r=-\infty}^{\infty} W_{pqr}(t) e^{-i(p+2q+3r)\omega_{800}t - i(q+r)\varphi - ir\gamma}, \quad (2)$$

where the Fourier coefficients $W_{pqr}(t)$ are given by the integral

$$W_{pqr}(t) = \frac{1}{8\pi^3} \int_{-\pi}^{\pi} \int_{-\pi}^{\pi} \int_{-\pi}^{\pi} w(F(t)|\mathcal{E}_{800} \cos \psi_{800} + \mathcal{E}_{400} \cos \psi_{400} + \mathcal{E}_{266} \cos \psi_{266}|) \times e^{ip\psi_{800} + iq\psi_{400} + ir\psi_{266}} d\psi_{800} d\psi_{400} d\psi_{266}. \quad (3)$$

Note that due to w being an even function of phases, $W_{pqr} \equiv 0$ for odd $p+q+r$. For even $p+q+r$, one can estimate the previous integral by smoothly approximating the steep function $w(|E|)$ by an exponential function, $w(|E|) \approx w(\mathcal{E}_m F) e^{n(|E|/\mathcal{E}_m F - 1)}$, where $\mathcal{E}_m = \mathcal{E}_{800} + \mathcal{E}_{400} + \mathcal{E}_{266}$ is the maximum total electric field and $n = w'(\mathcal{E}_m F) \mathcal{E}_m F / w(\mathcal{E}_m F) = 2\kappa^3 E_a / 3\mathcal{E}_m F - 1$ is the effective exponent of the dependence $w(|E|)$ at point $|E| = \mathcal{E}_m F$. With the use of this approximation, integral (3) can be evaluated for even $p+q+r$ as

$$W_{pqr}(t) \approx 2w(\mathcal{E}_m F) e^{-n} I_p \left(\frac{n\mathcal{E}_{800}}{\mathcal{E}_m} \right) I_q \left(\frac{n\mathcal{E}_{400}}{\mathcal{E}_m} \right) I_r \left(\frac{n\mathcal{E}_{266}}{\mathcal{E}_m} \right), \quad (4)$$

where $I_k(z)$ denotes the modified Bessel function of order k and argument z . For sufficiently long pulses, when ionization continues over several periods of the fundamental harmonic, the period-averaged ionization rate \bar{w} is determined only by terms with $p+2q+3r=0$ in sum (2). Such terms could be nonzero only for even $q=2s$, which allows us to rewrite the period-averaged ionization probability (2) as double sum

$$\bar{w}(t) \approx \sum_{r=0}^{\infty} \sum_{s=-\infty}^{\infty} (2 - \delta_{r0}) W_{|3r+4s|, 2|s|, |r|}(t) \times \cos[r\gamma + (r+2s)\varphi], \quad (5)$$

where δ_{jk} is the Kronecker delta.

Each term in sum (5) corresponds to a different parametric channel of ionization [26,27], that is, to a different way to represent zero frequency as a combination of frequencies ω_{800} , $2\omega_{800}$, and $3\omega_{800}$ with an even sum of coefficients. Since the coefficients W_{pqr} decrease quickly with their indices, only a few terms in (5) contribute significantly to the period-averaged ionization rate. Under the usual experimental conditions when both second and third harmonics are weaker than the fundamental ones, only four channels provide main contributions, $r=0, s=0, 1$ and $r=1, s=0, -1$, which gives

$$\bar{w} \approx W_{0,0,0} + 2W_{4,2,0} \cos(2\varphi) + 2W_{3,0,1} \cos(\varphi + \gamma) + 2W_{1,2,1} \cos(\varphi - \gamma). \quad (6)$$

The first term $W_{0,0,0}$ describes the main phase-independent background and is present even without the second and third harmonics. The other three terms give the modulation

of ionization rate which is consistent both the phase dependences observed in our experiments and the transitions between them when changing the intensity ratios $I^{(400)}/I^{(800)}$ and $I^{(266)}/I^{(800)}$.

Evaluating modified Bessel functions in Eq. (4) numerically for $\mathcal{E}_{400}/\mathcal{E}_{800} < 1$, $\mathcal{E}_{266}/\mathcal{E}_{800} < 0.5$, and $5 < n < 20$, one finds that $W_{4,2,0} \gg W_{1,2,1} + W_{3,0,1}$ for $\mathcal{E}_{266}/\mathcal{E}_{800} \ll (10 + 5\mathcal{E}_{800}^2/\mathcal{E}_{400}^2 n)^{-1}$ and vice versa $W_{4,2,0} \ll W_{1,2,1} + W_{3,0,1}$ for $\mathcal{E}_{266}/\mathcal{E}_{800} \gg (10 + 5\mathcal{E}_{800}^2/\mathcal{E}_{400}^2 n)^{-1}$. For the common experimental situations of ionization of molecules with ionization potential around 10–15 eV by pulses with total intensity of the level of 10^{14} W/cm², one has $n \approx 10$. Thus, if the third harmonic is absent or weak enough, $I^{(266)}/I^{(800)} \ll (10 + I^{(800)}/2I^{(400)})^{-2}$, then the modulation of ionization rate with phases is rather small and depends only on the phase shift φ of the second harmonic. The ionization rate is π periodic over φ , which is manifested as the peak at 1.43 PHz in Fig. 3(c) and explains naturally the fact that only this one peak at 1.43 PHz is observed for two-color pumping. In the opposite case, $I^{(266)}/I^{(800)} \gg (10 + I^{(800)}/2I^{(400)})^{-2}$, the second term in Eq. (6) is neglectable and the modulation of ionization rate is determined by the last two terms, appearing much stronger than in the two-color case without third harmonic. Among these two terms, the former, $2W_{3,0,1} \cos(\varphi + \gamma)$, is associated with joint ionization by the fundamental and third harmonics and is almost unaffected by second harmonic, whereas the latter, $2W_{1,2,1} \cos(\varphi - \gamma)$, requires the presence of all three colors and depends significantly on $I^{(400)}$. Therefore, the ratio $W_{3,0,1}/W_{1,2,1}$ depends significantly on $I^{(400)}/I^{(800)}$: for a not too strong second harmonic (with $I^{(400)}/I^{(800)} \lesssim 0.3$), $W_{3,0,1} > W_{1,2,1}$ holds and the 2D phase dependence is tilted left as in Figs. 4(a) and 4(d) and 5(a) and 5(d); for the stronger second harmonics, $W_{3,0,1} < W_{1,2,1}$, the phase dependence is tilted right as in Figs. 4(c) and 4(f) and Figs. 5(c) and 5(f). Note that the contributions in the ionization rate modulation from the second and third harmonics become comparable already at very low $I^{(266)} < 0.01I^{(800)}$ and $I^{(266)} \ll I^{(400)}$. Note also that the third harmonic results in 2π -periodic modulation, i.e., period doubling as compared to the two-color case, due to the breaking the mirror symmetry in the three-color fields, which is manifested as the peak at 0.75 PHz in Fig. 3(c) of the two upper curves. Such period doubling is very similar to the one observed previously in the phase dependencies of the amplitude of generated THz radiation [19].

We also solved the ionization equation numerically and calculated the final ionization degree $\sigma_f = N(t \rightarrow +\infty)/N_g$ created by the three-color field (1). In the calculations below, we use the formula in Refs. [13,17,19,28] for the ionization rate of the molecular nitrogen, $w(|E|) = 4\omega_a \kappa^5 (E_a/|E|) \exp(-2\kappa^3 E_a/3|E|)$, where $\omega_a \approx 4.13 \times 10^{16}$ s⁻¹ and $E_a \approx 5.14 \times 10^9$ V/cm are the atomic units of frequency and field strength, respectively, and $\kappa = \sqrt{U_{N_2}/U_H}$, with $U_H = 13.6$ eV and $U_{N_2} = 15.6$ eV being the ionization potentials of atomic hydrogen and molecular nitrogen, respectively.

The calculated dependencies of σ_f on φ and γ are presented in Fig. 7 and are consistent with both the experimental results shown in Figs. 4(a)–4(c) and the analytical Eqs. (4)–(6). Figures 7(a)–7(c) correspond to the three-color pulses

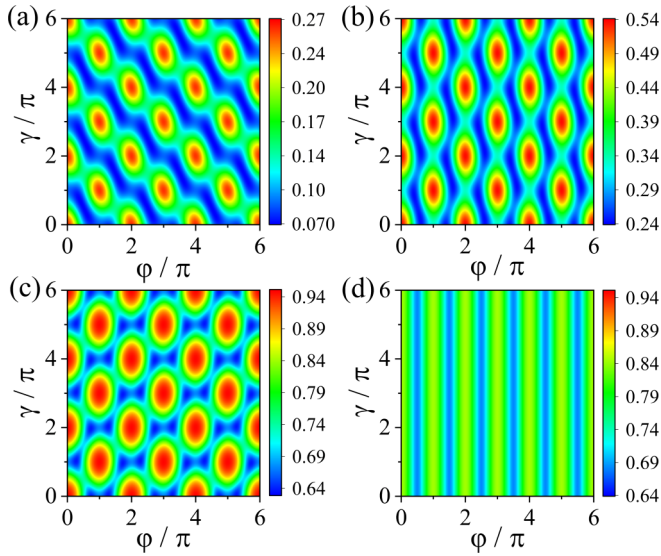


FIG. 7. Calculated ionization degree of nitrogen molecules as a function of the relative phases. (a)–(c) The intensity of the 800-nm laser field is 1.5×10^{14} W/cm², and the intensity ratios between the 800-, 400-, and 266-nm pulses are 1: 0.05: 0.008, 1: 0.16: 0.004, and 1: 0.4: 0.017 for (a)–(c), respectively. In (d), the intensity of the 266-nm pulses is set to be 0 and the other parameters are the same as those of (c).

with the same intensity ratios as estimated for Figs. 4(a)–4(c), and Fig. 7(d) presents results for the two-color field with the same intensities of the 800- and 400-nm field as in Fig. 7(c). The modulation in three-color cases is much stronger compared to the two-color case in Fig. 7(d) in agreement with the experimental observations presented in Fig. 3(b) and analytical formulas obtained for contributions of different parametric channels. This also can be seen from Fig. 8 which shows the calculated modulation depth in σ_f (difference between maximum and minimum over on φ and γ) as a function of $I^{(400)}$ and $I^{(266)}$. As seen, the modulation depth may reach tens of percent, resulting in a strong enhancement or suppression of ionization. Although the second harmonic alone (without the third one) is unable to induce strong modulation, it can significantly enhance the control effect from the third harmonic, which makes the three-color pulses containing both the second and third harmonics more advantageous for coherent ionization control than the two-color pulses.

In summary, we investigated the ionization of gas molecules in air by an intense femtosecond laser field consisting of a fundamental frequency and second and third harmonics. It was found that the ionization rates of both the HOMO and the HOMO-2 of nitrogen molecules depend sensitively on the relative phases between the three colors. For different intensity ratios between the 400- and 800-nm pulses, the ionization shows a different dependence on the two phases, manifesting as 2D “strips” tilted left or right. We simulated the ionization process driven by multiple color laser fields in the tunnel regime and revealed that the ionization rate is determined by a series of multiwave mixing terms

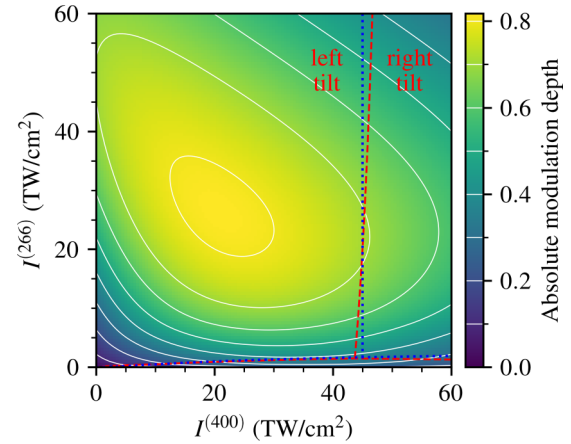


FIG. 8. Calculated modulation depth of the final ionization degree produced by the three-color pulse ionizing nitrogen gas as a function of the second- and third-harmonic intensities, $I^{(400)}$ and $I^{(266)}$. The heat map shows the absolute modulation (difference between the maximum and minimum ionization degree over phase shifts $\Delta\varphi$ and $\Delta\gamma$), and the white solid curves are the level lines. The blue dotted line and red dashed line mark the boundaries of the regions where different parametric channels are prominent, manifesting in different 2D phase diagrams with dominant dependence (i) on the phase sum $\Delta\varphi + \Delta\gamma$ (“left tilt”), (ii) on the difference $\Delta\varphi - \Delta\gamma$ (“right tilt”), or (iii) on the doubled phase $2\Delta\varphi$ (narrow region along horizontal axis). The blue dotted lines plotted using analytical conditions derived: $I^{(400)}/I^{(800)} = 0.3$ and $I^{(266)}/I^{(800)} = (10 + I^{(800)}/2I^{(400)})^{-2}$, and the red dashed lines are obtained numerically by comparing the corresponding Fourier components of the calculated phase dependencies. The fundamental-field intensity is fixed at $I^{(800)} = 1.5 \times 10^{14}$ W/cm² and pulse duration is $\tau_p = 35$ fs.

(parametric channels of ionization). Depending on the relative strength of the laser fields, the maximum ionization rate can be dominated by different wave mixing terms, in good agreement with our experimental observations. The control of strong field ionization rates by a three-color scheme is general and can be applied to other atomic and molecular gases besides to air. Therefore, the possibility of adjusting the ionization rate by changing the phase structure of the ionizing field opens different ways to control and optimize laser-matter interactions.

The work was supported in part by the National Natural Science Foundation of China (Grants No. 12034013, No. 11604205, and No. 11904232), Innovation Program of Shanghai Municipal Education Commission (Grant No. 2017-01-07-00-07-E00007), Open Fund of the State Key Laboratory of High Field Laser Physics (Shanghai Institute of Optics and Fine Mechanics), and “The Belt and Road Initiative” international collaboration project of Shanghai Municipal Commission of Science and Technology (Grant No. 19560745800). C.L. acknowledges support from the Talent Program of Shanghai University of Engineering Science. V.A.K. acknowledges support from the Russian Science Foundation (Grant No. 18-11-00210, analytical model).

- [1] M. Hentschel, R. Kienberger, C. Spielmann, G. A. Reider, N. Milosevic, T. Brabec, P. Corkum, U. Heinzmann, M. Drescher, and F. Krausz, Attosecond metrology, *Nature* **414**, 509 (2001).
- [2] A. Couairon and A. Mysyrowicz, Femtosecond filamentation in transparent media, *Phys. Rep.* **441**, 47 (2007).
- [3] B. Forestier, A. Houard, I. Revel, M. Durand, Y. B. André, B. Prade, A. Jarnac, J. Carbonnel, M. L. Nevé, J. C. d. Miscault *et al.*, Triggering, guiding and deviation of long air spark discharges with femtosecond laser filament, *AIP Adv.* **2**, 012151 (2012).
- [4] X. Xie, J. Dai, and X.-C. Zhang, Coherent Control of THz Wave Generation in Ambient Air, *Phys. Rev. Lett.* **96**, 075005 (2006).
- [5] A. Mitrofanov, D. Sidorov-Biryukov, M. Nazarov, A. Voronin, M. Rozhko, A. Fedotov, and A. Zheltikov, Coherently enhanced microwave pulses from midinfrared-driven laser plasmas, *Opt. Lett.* **46**, 1081 (2021).
- [6] L. Jiang, A.-D. Wang, B. Li, T.-H. Cui, and Y.-F. Lu, Electrons dynamics control by shaping femtosecond laser pulses in micro/nanofabrication: Modeling, method, measurement and application, *Light Sci. Appl.* **7**, 17134 (2018).
- [7] M. Burger, P. J. Skrodzki, L. A. Finney, J. Nees, and I. Jovanovic, Remote detection of uranium using self-focusing intense femtosecond laser pulses, *Remote Sens.* **12**, 1281 (2020).
- [8] E. Papastathopoulos, M. Strehle, and G. Gerber, Optimal control of femtosecond multiphoton double ionization of atomic calcium, *Chem. Phys. Lett.* **408**, 65 (2005).
- [9] L. Englert, B. Rethfeld, L. Haag, M. Wollenhaupt, C. Sarpe-Tudoran, and T. Baumert, Control of ionization processes in high band gap materials via tailored femtosecond pulses, *Opt. Express* **15**, 17855 (2007).
- [10] A. Castro, E. Räsänen, A. Rubio, and E. Gross, Femtosecond laser pulse shaping for enhanced ionization, *Europhys. Lett.* **87**, 53001 (2009).
- [11] J. Plenge, A. Wirsing, I. Wagner-Drebenstedt, I. Halfpap, B. Kieling, B. Wassermann, and E. Rühl, Coherent control of the ultrafast dissociative ionization dynamics of bromochloroalkanes, *Phys. Chem. Chem. Phys.* **13**, 8705 (2011).
- [12] N. Shvetsov-Shilovski, L. Madsen, and E. Räsänen, Suppression of strong-field ionization by optimal pulse shaping: Application to hydrogen and the hydrogen molecular ion, *Phys. Rev. A* **91**, 023425 (2015).
- [13] D. Schumacher and P. Bucksbaum, Phase dependence of intense-field ionization, *Phys. Rev. A* **54**, 4271 (1996).
- [14] P. Béjot, G. Karras, F. Billard, E. Hertz, B. Lavorel, E. Cormier, and O. Faucher, Harmonic Generation and Nonlinear Propagation: When Secondary Radiations Have Primary Consequences, *Phys. Rev. Lett.* **112**, 203902 (2014).
- [15] D. Jang, R. M. Schwartz, D. Woodbury, J. Griff-McMahon, A. H. Younis, H. M. Milchberg, and K.-Y. Kim, Efficient terahertz and Brunel harmonic generation from air plasma via mid-infrared coherent control, *Optica* **6**, 1338 (2019).
- [16] L. E. Chipperfield, J. S. Robinson, J. W. G. Tisch, and J. P. Marangos, Ideal Waveform to Generate the Maximum Possible Electron Recollision Energy for Any Given Oscillation Period, *Phys. Rev. Lett.* **102**, 063003 (2009).
- [17] P. G. de Alaiza Martínez, I. Babushkin, L. Bergé, S. Skupin, E. Cabrera-Granado, C. Köhler, U. Morgner, A. Husakou, and J. Herrmann, Boosting Terahertz Generation in Laser-Field Ionized Gases Using a Sawtooth Wave Shape, *Phys. Rev. Lett.* **114**, 183901 (2015).
- [18] V. Kostin and N. Vvedenskii, Generation of Few-And Subcycle Radiation in Midinfrared-To-Deep-Ultraviolet Range During Plasma Production by Multicolor Femtosecond Pulses, *Phys. Rev. Lett.* **120**, 065002 (2018).
- [19] S. Liu, Z. Fan, C. Lu, J. Gui, C. Luo, S. Wang, Q. Liang, B. Zhou, A. Houard, A. Mysyrowicz *et al.*, Coherent control of boosted terahertz radiation from air plasma pumped by a femtosecond three-color sawtooth field, *Phys. Rev. A* **102**, 063522 (2020).
- [20] P. Wei, J. Miao, Z. Zeng, C. Li, X. Ge, R. Li, and Z. Xu, Selective Enhancement of a Single Harmonic Emission in a Driving Laser Field with Subcycle Waveform Control, *Phys. Rev. Lett.* **110**, 233903 (2013).
- [21] Y. Kida, K. Sakamoto, and T. Imasaka, High-energy multicolor femtosecond pulses in the deep-ultraviolet generated through four-wave mixing induced by three-color pulses, *App. Phys. B* **122**, 214 (2016).
- [22] S. Mityukovskiy, Y. Liu, P. Ding, A. Houard, A. Couairon, and A. Mysyrowicz, Plasma Luminescence from Femtosecond Filaments in Air: Evidence for Impact Excitation with Circularly Polarized Light Pulses, *Phys. Rev. Lett.* **114**, 063003 (2015).
- [23] R. Danylo, X. Zhang, Z. Fan, D. Zhou, Q. Lu, B. Zhou, Q. Liang, S. Zhuang, A. Houard, A. Mysyrowicz *et al.*, Formation Dynamics of Excited Neutral Nitrogen Molecules inside Femtosecond Laser Filaments, *Phys. Rev. Lett.* **123**, 243203 (2019).
- [24] S. I. Mityukovskiy, Y. Liu, A. Houard, and A. Mysyrowicz, Re-evaluation of the peak intensity inside a femtosecond laser filament in air, *J. Phys. B: At. Mol. Opt. Phys.* **48**, 094003 (2015).
- [25] H. Guo, T.-J. Wang, X. Zhang, C. Liu, N. Chen, Y. Liu, H. Sun, B. Shen, Y. Jin, Y. Leng *et al.*, Direct measurement of radial fluence distribution inside a femtosecond laser filament core, *Opt. Express* **28**, 15529 (2020).
- [26] V. A. Kostin and N. V. Vvedenskii, Mutual enhancement of Brunel harmonics, *JETP Lett.* **110**, 457 (2019).
- [27] L. Li, P. Lan, L. He, X. Zhu, J. Chen, and P. Lu, Scaling Law of High Harmonic Generation in the Framework of Photon Channels, *Phys. Rev. Lett.* **120**, 223203 (2018).
- [28] P. Corkum, N. Burnett, and F. Brunel, Above-Threshold Ionization in the Long-Wavelength Limit, *Phys. Rev. Lett.* **62**, 1259 (1989).